arXiv:1204.3393v1 [astro-ph.CO] 16 Apr 2012

Limitations in Determining Equation of State of Dark Energy at High Redshift

Qiping Su[1*] and Rong-Gen Cai[2†]

[1] *Department of Physics, Hangzhou Normal University, Hangzhou, 310036, China*

[2] *State Key Laboratory of Theoretical Physics,*
Institute of Theoretical Physics, Chinese Academy of Sciences,
P.O. Box 2735, Beijing 100190, China

(Dated: March 2, 2013)

Abstract

By dividing the redshift region under consideration into two bins, we estimate the limitations in determining the equation of state w_{de} of dark energy at high redshift from current and future observational data including supernovae, baryon acoustic oscillation and observational Hubble data. It is found that the constraints of w_{de} from current data are weak ($2\sigma(w_{de}) \sim 1$) even beyond redshift $z = 0.3$. For simulated future observational data, it is shown that ~ 2300 supernovae data from a SANP-like JDEM survey give $2\sigma(w_{de}) \sim 1$ beyond $z = 0.6$. We consider the effects of the divided point, the number of supernovae data and the error in the distance modulus on constraining w_{de} at high redshift. It is shown that the increase of number of supernovae data seems not efficient on improving the constraints of w_{de} at high redshift, while the improvement of observational error in distance modulus seems to be a better way.

---

*Electronic address: sqp@hznu.edu.cn

†Electronic address: cairg@itp.ac.cn

I. INTRODUCTION

The current expansion of the universe is found to be in accelerating [1, 2] and it is believed that the dark energy (DE), whose equation of state $w_{de} = p_{de}/\rho_{de}$ is less than $-1/3$, plays the role to drive the accelerated expansion of the universe. Plenties of DE models have been proposed [3–9] but the origin of DE is still unknown. One has only known a little about DE from observational data. Several parametrization methods of w_{de} have been proposed to fit with observations to get constraints of w_{de}. Usually in parametrization w_{de} is assumed to be a simple function of redshift z, e.g., the CPL parametrization [10, 11]: $w_{de}(z) = w_0 + w_a z/(1+z)$, and the parametrization of redshift expansion [12, 13]: $w_{de}(z) = w_0 + w_z z$. It has been found that w_{de} is very close to -1 at low redshift and is varying very slowly (if it is dynamical). Of course the fitting results depend on the parametrization forms of $w_{de}(z)$. And an assumed form of $w_{de}(z)$ might be only suitable to describe one type of w_{de}. For example, the CPL parametrization cannot describe the equation of state with oscillations or rapid transitions. In general, one parametrization form of $w_{de}(z)$ could only approximate the real w_{de} well in a very limited region of redshift.

Several model-independent methods have also been proposed to reconstruct $w_{de}(z)$ from observational data [14–17], e.g., uncorrelated band-power estimates (UBE) [18, 19], cubic-spline method [20], linear-spline method [21],wavelet approach [22], and so on. Most of these methods relate to a piecewise $w_{de}(z)$:

$$w_{de}(z) = w_i(z) \ , \quad z_i < z \leq z_{i+1} \ , \tag{1}$$

where $z_0 = 0$ and $w_i(z)$ is a simple function of redshift z in the i^{th} bin. It is not surprising that in higher redshift bins, constraints of w_{de} from observational data will be weaker [23]. There are mainly two reasons: 1) In higher redshift bins the number of currently available data points will be much less. At present, the most data points to constrain DE are from Type Ia supernovae (SnIa). There are much less SnIa data points in higher redshift bins, as shown in Table I. Moreover, w_{de} in one bin can also be constrained by data points of other bins that have higher redshift, i.e., w_{de} in the lowest redshift bin can be constrained by all data points. 2) In higher redshift bins, the fractional energy density of DE $\Omega_{de} = \rho_{de}/3H^2$ is always be smaller than the one of dark matter, so the role played by DE in the luminosity

z→	0.2	0.4	0.6	0.8	1.0	1.2	1.4
N_{bin}	173	77	71	78	60	8	5

TABLE I: The redshift distribution of 472 supernovae data from 3 years Supernova Legacy Survey. The redshifts in the first row are the upper limits of each bin.

distance

$$D_l(z) = (1+z)\int_0^z dx/H(x) \tag{2}$$

will be weaker. This can be seen in a simple calculation as follows. In a flat FRW universe the Fridemann equation reads:

$$H^2(x) = \frac{1}{3}[\rho_{m0}(1+x)^3 + \rho_{de}(x)], \tag{3}$$

where

$$\rho_{de}(x) = \rho_{de0} e^{3\int_0^x \frac{1+w_{de}(y)}{1+y}dy}. \tag{4}$$

Supposing there is a tiny variation δw_i of w_{de} in the i^{th} bin and no variations of w_{de} in all other bins, from Eq.(2) and (3) one has

$$\delta H^2(x) = \begin{cases} 0 \ , & 0 \le x \le z_i \\ \rho_{de}\ln\left(\frac{1+x}{1+z_i}\right)\delta w_i \ , & z_i < x \le z_{i+1} \\ \rho_{de}\ln\left(\frac{1+z_{i+1}}{1+z_i}\right)\delta w_i \ , & z_{i+1} < x \end{cases} \tag{5}$$

and correspondingly

$$\delta D_l(z) = \begin{cases} 0 \ , & 0 \le z \le z_i \\ -\frac{3}{2}(1+z)\int_{z_i}^z \frac{\delta w_i}{H(x)}\Omega_{de}\ln\left(\frac{1+x}{1+z_i}\right)dx \ , & z_i < z \le z_{i+1} \\ -\frac{3}{2}(1+z)\left[\int_{z_i}^{z_{i+1}} \frac{\delta w_i}{H(x)}\Omega_{de}\ln\left(\frac{1+x}{1+z_i}\right)dx + \int_{z_{i+1}}^{z} \frac{\delta w_i}{H(x)}\Omega_{de}\ln\left(\frac{1+z_{i+1}}{1+z_i}\right)dx\right] \ , & z_{i+1} < z \end{cases} \tag{6}$$

We can see that δw_i always appears together with Ω_{de} in $\delta D_l(z)$. Since Ω_{de} is much smaller at higher redshift, $\delta D_l(z)$ is also a smaller change in higher redshift bins with the same δw_i, i.e., $\delta D_l(z)$ will be less sensitive to δw_i. It indicates that when the redshift in a bin is larger (i is larger), to lead to the same variation of D_l the change of w_i must be larger. In other words, the constraint on w_{de} from the luminosity distance is weaker in higher redshift bins than in lower redshift ones.

As shown in Eq.(6), δD_l in the i^{th} bin is an integration, which is mainly effected by evolving of Ω_{de} with z and the width of this bin. At high redshift bins Ω_{de} will be small and

$$\Omega_{de}(z_i < z < z_{i+1}) \sim (1+z)^{3w_i} \ . \tag{7}$$

When w_i is larger and the bin is wider, δD_l in the i^{th} bin will be larger. There is a situation which needs to be mentioned that at a high redshift bin if w_i is much smaller than -1, the decrease of Ω_{de} will be so rapid that δD_l keeps extremely small even the bin is very wide and δw_i is very large. In this case, the likelihood of w_i will be very flat in a large region of small w_i as shown in Fig. 2 in the next section, since w_i in this large region almost has the same D_l. Thus the downward errors of w_i at high redshift bins are always extremely large. In general, the constraint of w_{de} in the last redshift bin is always the weakest and the downward error of w_{de} is always very big.

In this paper, we would like to estimate the limitations in determining w_{de} at high redshift from present and future observational data. Constraints of w_{de} will be obtained by using the UBE method with 2 redshift bins and errors of w_{de} in the second bin indicate the limitations in determining w_{de} at high redshift. The effects of divided positions of two redshift bins, the number of SnIa data and observational error of SnIa data in constraining w_{de} at high redshift will be studied.

II. CONSTRAINTS OF w_{de} FROM PRESENT DATA

We will use the UBE method to get constraints of w_{de} from 472 Supernova Legacy Survey 3 years data (SNLS3)[24], Baryon Acoustic Oscillation (BAO) Distance Parameter A [25] and 12 Observational Hubble Data with $z < 1.4$ from [26–28]. In this case, redshift for all those data points are smaller than 1.4 and one needs not to involve w_{de} in higher redshift region with $z > 1.4$. In Table II, 12 Hubble data are listed. And the BAO Distance Parameter A is defined as:

$$A = \Omega_{m0}^{1/2} E^{-1/3}(0.35) \left(\frac{1}{0.35} \int_0^{0.35} \frac{dz}{E(z)} \right)^{2/3} , \tag{8}$$

where $E(z) \equiv H(z)/H(0)$ and $\Omega_{m0} \equiv \rho_{m0}/3H^2(0)$. The redshift region of $[0, 1.4]$ will be divided into two bins and

$$w_{de}(z) = \begin{cases} w_1 \ , & 0 \le z \le z_1 \\ w_2 \ , & z_1 < z \le 1.4 \end{cases} , \tag{9}$$

z	0	0.1	0.17	0.27	0.4	0.48	0.88	0.9	1.3	0.24	0.34	0.43
h	0.738	0.69	0.83	0.77	0.95	0.97	0.9	1.17	1.68	0.7969	0.838	0.8645
σ_h	0.024	0.12	0.08	0.14	0.17	0.6	0.4	0.23	0.17	0.0232	0.0296	0.0327

TABLE II: 12 observational Hubble data with their redshifts $z < 1.4$ from [26–28].

where w_1 and w_2 are two constants. The divided position z_1 will be set as 0.3, 0.35, 0.4 and 0.45, respectively, as shown in Fig. 1. The best-fitted parameters and their 68.3%, 95.4% confidence level (C.L.) errors are obtained by using the Markov chain Monte Carlo (MCMC) method, which are shown in Table III. The errors of w_2 can be used to estimate the limitations in determining w_{de} beyond $z = z_1$. In the numerical calculation we have set the prior with $w_2 > -20$, or w_2 would go to a very large minus value in MCMC procedure and the downward error of w_2 would be extremely large, as discussed in the introduction. The figure of merit (FoM) defined as [29, 30]:

$$\text{FoM} = [\det C(w_1, w_2)]^{-1/2} \ , \tag{10}$$

has also been calculated for each model, where $C(w_0, w_1)$ is the covariance matrix of w_1 and w_2 after marginalizing out all other parameters of the model. Moreover, it is found that the correlation between w_1 and w_2 is very small, i.e., the errors of w_1 and w_2 obtained can be treated as independent with each other.

z_1	Ω_{m0}	w_1	w_2	χ^2_{min}	FoM
0.30	$0.279^{+0.023+0.047}_{-0.020-0.040}$	$-1.05^{+0.09+0.19}_{-0.10-0.21}$	$-1.44^{+0.42+0.74}_{-0.54-1.19}$	423.988	19.346
0.35	$0.277^{+0.031+0.055}_{-0.016-0.038}$	$-1.08^{+0.09+0.19}_{-0.09-0.19}$	$-1.52^{+0.62+1.01}_{-0.87-2.39}$	424.323	11.525
0.40	$0.272^{+0.042+0.067}_{-0.010-0.033}$	$-1.11^{+0.11+0.21}_{-0.07-0.17}$	$-1.31^{+0.78+1.12}_{-2.35-7.87}$	424.614	4.115
0.45	$0.269^{+0.045+0.067}_{-0.006-0.029}$	$-1.09^{+0.07+0.16}_{-0.12-0.21}$	$-0.92^{+0.79+0.90}_{-6.80-19.07}$	424.764	1.981

TABLE III: The best-fitted values and their 68.3% and 95.4% C.L. errors of the UBE models from present observational data. In the UBE models, the redshift region (0, 1.4) is divided into two bins and the divided positions are $z_1 = 0.3, 0.35, 0.4, 0.45$, respectively. The figure of merit in each case is also calculated.

From the above we may conclude as follows.

1. When the redshift region of the second bin becomes smaller, the constraints of w_2 then become much weaker. As shown in Fig. 1, the errors of w_2 increase very rapidly with

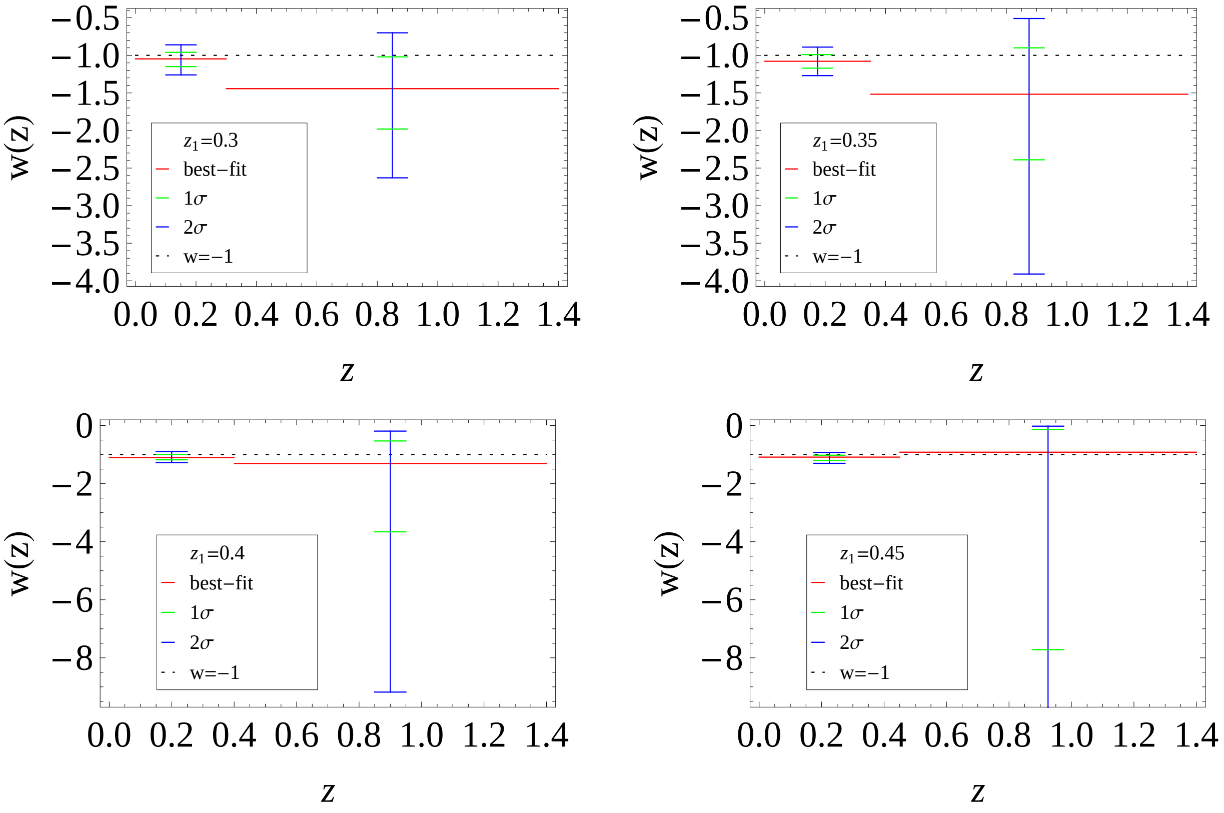

FIG. 1: The best-fitted $w_{de}(z)$ and its 68.3% and 95.4% C.L. errors of the UBE models from the present observational data.

the divided point z_1. It is shown in Table III that the errors of w_{de} beyond $z_1 = 0.3$ is large (the width of uncertainty of w_2 at 95.4% C.L. is 1.93, i.e., $2\sigma(w_2) \sim 1$), compared with the ones with $z < 0.3$. Furthermore, if one sets up $z_1 > 0.45$, the constraints of w_{de} beyond z_1 will be extremely large (its lower limit at 95.4% C.L. is smaller than -20). Therefore it is very hard to determine w_{de} at high redshift from current observational data.

2. At high redshift, the likelihood of w_{de} is flat on its downward side. As shown in Fig. 2, for larger z_1 the likelihood of w_2 is flatter on the downward side, and thus the downward errors of w_2 are much larger, as shown in Fig. 1.

3. The effect of the divided point z_1 on w_1, i.e., w_{de} in low redshift region, is very small. With very different z_1 there is a little difference between the errors of corresponding w_1, as shown in Table III and Fig. 1. It indicates that the number of present data at low redshift is sufficient and constraints on w_{de} in this region is strong.

4. FoM can be used to estimate the goodness of constraints of w_{de} at high redshift from

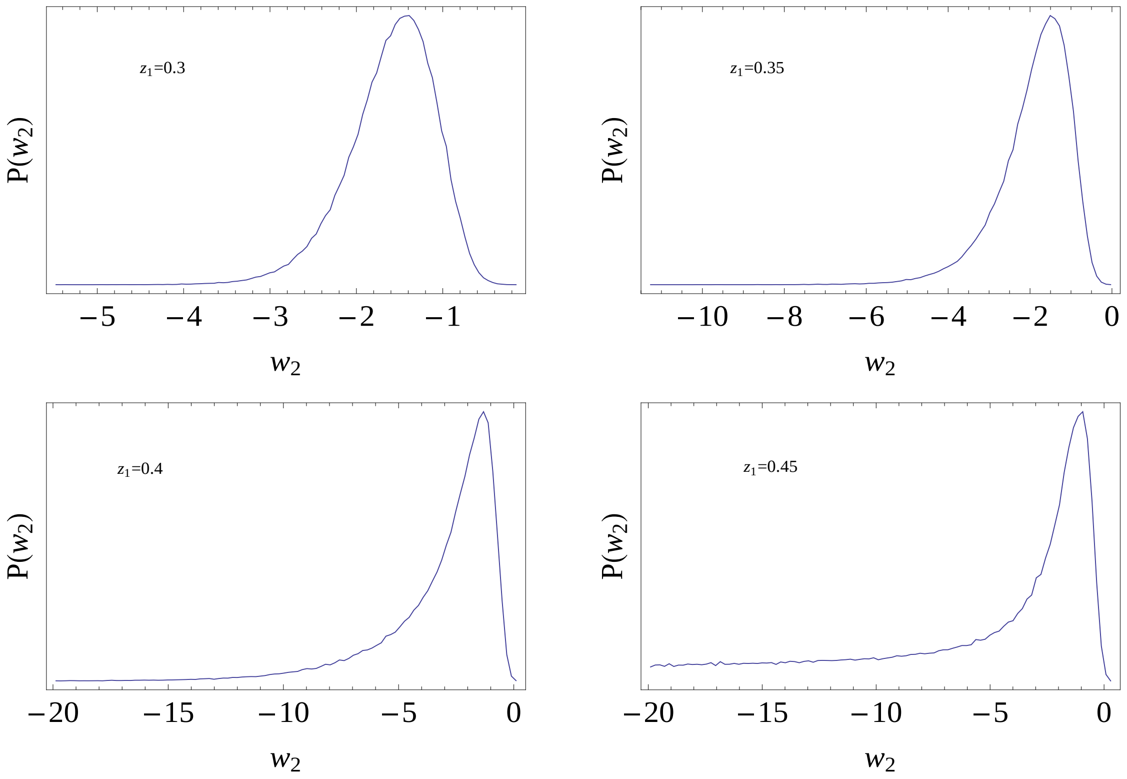

FIG. 2: The likelihood of w_2 of the UBE models with the divided points $z_1 = 0.3, 0.35, 0.4, 0.45$, respectively.

z→	0.1	0.2	0.3	0.4	0.5	0.6	0.7	0.8	0.9	1.0	1.1	1.2	1.3	1.4	1.5	1.6	1.7
N_{bin}	300	35	64	95	124	150	171	183	179	170	155	142	130	119	107	94	80

TABLE IV: The redshift distribution of 1998 SN data for a SNAP-like JDEM survey and 300 SN data from the NSNF [31, 32]. The redshifts in the first row are the upper limits of each bin.

observations. FoM from Eq.(10) is proportional to the inverse area of the error ellipse in the $w_1 \sim w_2$ plane. Since errors of w_1 change very slowly with z_1, differences between FoM with different z_1 are mainly from differences between the errors of w_2. FoM can be used to estimate the effect of z_1 on constraints of w_2, i.e., the goodness of constraints of w_{de} beyond $z = z_1$. As shown in Table III, FoM increases rapidly with the decrease of z_1.

III. CONSTRAINTS OF w_{de} FROM FUTURE DATA

To estimate the constraints of w_{de} at high redshift from future observations, we will fit the 2-binned UBE model shown in Eq.(9) with 2298 simulated supernovae data (denoted as elementary data set in this paper), which contain 1998 supernovae data with $0.1 < z < 1.7$ from a SNAP-like JDEM survey and 300 supernovae data with $z < 0.1$ from the NSNF [31, 32]. The redshift distribution of the mock supernovae data is shown in Table IV. To alleviate the degeneracy between Ω_{m0} and w_{de}[33], the data of the BAO Distance Parameter A [25] will also be included. To simulate the mock supernovae data, we assume the fiducial model as $w_{de}(z) = -1$. The error in the distance modulus for each supernovae will be set as $\delta = 0.13$ [17], except in the subsection C. In this section we will study the effect of the position of z_1, the number of supernovae data and the value of δ in constraining w_{de} at high redshift.

A. The effects of the divided position of bins

z_1	Ω_{m0}	w_1	w_2	χ^2_{min}	FoM
0.4	$0.291^{+0.026+0.045}_{-0.014-0.035}$	$-0.96^{+0.03+0.07}_{-0.04-0.09}$	$-1.12^{+0.17+0.30}_{-0.24-0.55}$	2291.612	119.650
0.6	$0.285^{+0.030+0.053}_{-0.013-0.033}$	$-0.97^{+0.03+0.08}_{-0.06-0.12}$	$-1.14^{+0.27+0.45}_{-0.42-1.31}$	2292.223	33.231
0.8	$0.279^{+0.028+0.056}_{-0.012-0.030}$	$-0.96^{+0.04+0.08}_{-0.07-0.15}$	$-1.11^{+0.43+0.73}_{-0.69-4.03}$	2292.663	11.680
1.0	$0.275^{+0.032+0.048}_{-0.008-0.022}$	$-0.95^{+0.02+0.06}_{-0.08-0.15}$	$-1.11^{+0.89+1.28}_{-1.88-18.73}$	2292.802	5.885

TABLE V: The best-fitted values and their 68.3% and 95.4% C.L. errors of the UBE models from the 2298 simulated supernovae data. In the UBE models, the redshift region $(0, 1.7)$ is divided into two bins and the divided positions are $z_1 = 0.4, 0.6, 0.8, 1.0$, respectively. The figure of merit in each case is also included.

To estimate the effect of the divided position z_1 on errors of w_{de}, we have set z_1 as 0.4, 0.6, 0.8 and 1.0, respectively, as shown in Table V and Fig. 3. As expected, errors of w_{de} at high redshift (i.e., w_2) increase rapidly with z_1. One can see that constraints of w_{de} is weak beyond $z = 0.6$: in the case of $z_1 = 0.6$, the width of error region of w_2 at 95.4% C.L. is 1.76 (i.e., $2\sigma(w_2) \sim 1$), which is similar to the constraints of w_{de} beyond $z = 0.3$ from the current data (in the previous section). It also shows that constraints of w_{de} beyond $z = 1$ becomes extremely weak. On the other hand, the constraint on w_{de} at low redshift (w_1) will be much better than that from the present data. Finally one can see that the value of χ^2_{min} changes very slowly with z_1.

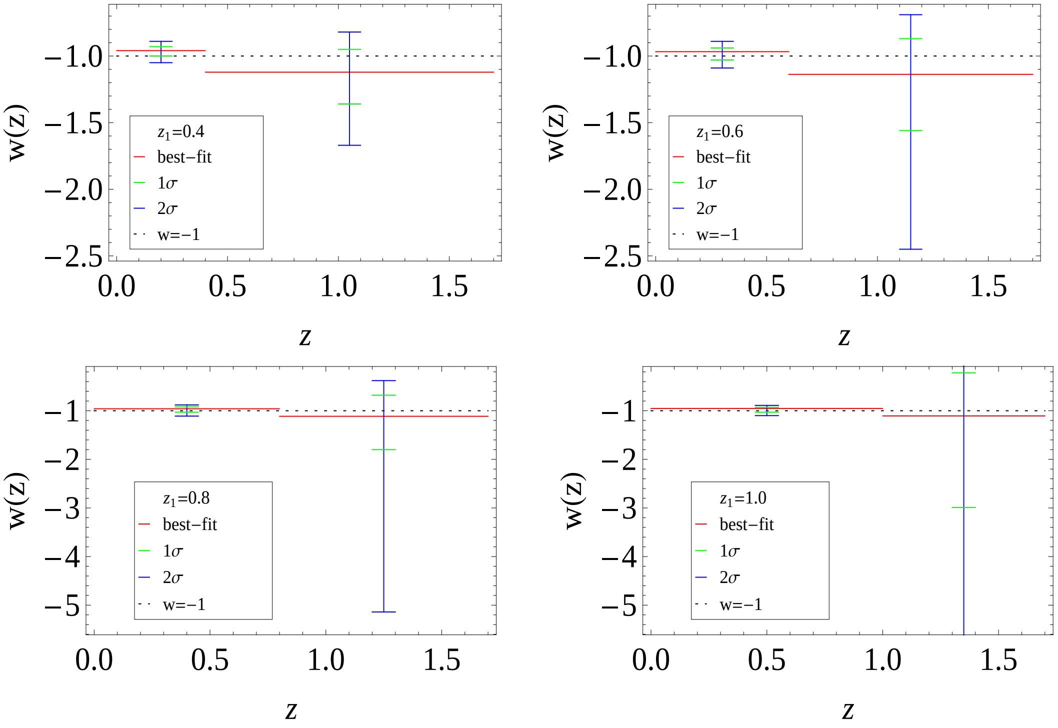

FIG. 3: Plots of the best-fitted $w_{de}(z)$ and their 68.3% and 95.4% C.L. errors shown in Table V.

B. The effects of the number of supernovae data

multiple	Ω_{m0}	w_1	w_2	χ^2_{min}	FoM
×2	$0.277^{+0.038+0.047}_{-0.008-0.018}$	$-0.96^{+0.03+0.06}_{-0.08-0.13}$	$-1.33^{+0.82+1.13}_{-1.95-18.64}$	4577.434	6.641
×3	$0.279^{+0.018+0.034}_{-0.008-0.020}$	$-1.00^{+0.02+0.06}_{-0.05-0.11}$	$-1.01^{+0.54+0.93}_{-0.86-3.48}$	6827.183	15.407
×4	$0.278^{+0.015+0.029}_{-0.007-0.020}$	$-1.00^{+0.03+0.06}_{-0.04-0.08}$	$-1.20^{+0.49+0.89}_{-0.72-2.49}$	9187.008	22.034
×5	$0.276^{+0.012+0.022}_{-0.008-0.017}$	$-0.99^{+0.02+0.05}_{-0.04-0.06}$	$-1.00^{+0.37+0.65}_{-0.47-1.27}$	11426.776	92.482

TABLE VI: The best-fitted values and their 68.3% and 95.4% C.L. errors of the UBE models from simulated supernovae data. The numbers of supernovae data are respectively $2, 3, 4$, and 5 times of the 2298 elementary data, respectively. In the UBE models, the redshift region $(0, 1.7)$ is divided into two bins and the divided position z_1 is set to 1.0. The figure of merit for each case is also calculated.

In the subsection A it is shown that ~ 2300 mock future supernovae data still give poor constraints of w_{de} beyond $z = 0.6$. Here we would like to see the effects if we increase the

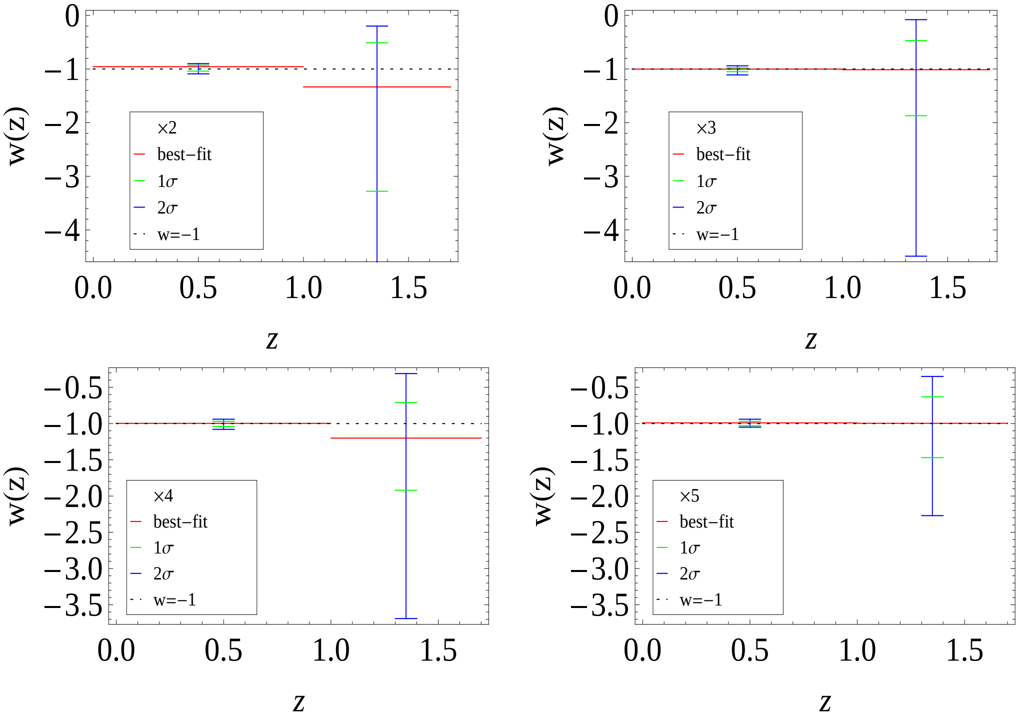

FIG. 4: Plots of the best-fitted $w_{de}(z)$ and their 68.3% and 95.4% C.L. errors shown in Table VI.

number of the mock supernovae data, with 2, 3, 4 and 5 times of the 2298 elementary data introduced in the subsection A. The proportional distribution of redshift in these multiple datasets is the same as the elementary data set, as shown in Table IV. The divided position of two bins z_1 is set to 1.0 . The results are shown in Table VI and Fig. 4. It shows that the improvement of FoM (i.e., constraints of w_{de} beyond $z = 1$) with increase of the number of data points is not very efficient. Constraints of w_{de} beyond $z = 1$ from the data with 5 times number of the elementary supernovae data set are still weak ($2\sigma(w_2) \sim 1$ with 5 times number of data).

C. The effects of the error in the distance modulus

One can see that increasing the number of supernovae data seems not efficient enough to improve constraints of w_{de} at high redshift. However, it is expected that with the increase of number of data, the statistical errors will be improved and the systematic errors should also be improved more and more by future observations [34]. To estimate effects of the error δ, here we set $\delta = 0.13, 0.1, 0.05, 0.02$, respectively. The number of the supernovae used here

δ	Ω_{m0}	w_1	w_2	χ^2_{min}	FoM
0.13	$0.279^{+0.018+0.034}_{-0.008-0.020}$	$-1.00^{+0.02+0.06}_{-0.05-0.11}$	$-1.01^{+0.54+0.93}_{-0.86-3.48}$	6827.183	15.407
0.10	$0.280^{+0.012+0.024}_{-0.007-0.018}$	$-1.00^{+0.01+0.05}_{-0.04-0.07}$	$-1.01^{+0.41+0.72}_{-0.55-1.52}$	6827.182	30.567
0.05	$0.280^{+0.006+0.012}_{-0.004-0.010}$	$-1.00^{+0.01+0.03}_{-0.01-0.04}$	$-1.01^{+0.22+0.39}_{-0.24-0.55}$	6827.182	386.480
0.02	$0.280^{+0.002+0.004}_{-0.001-0.004}$	$-1.00^{+0.00+0.00}_{-0.00-0.01}$	$-1.00^{+0.08+0.16}_{-0.09-0.19}$	6827.183	2478.160

TABLE VII: The best-fitted values and their 68.3% and 95.4% C.L. errors of the UBE models with errors in distance modulus $\delta = 0.13, 0.10, 0.05, 0.02$, respectively. The number of supernovae used is 3 times of 2298 elementary supernovae data. In the UBE model, the redshift region $(0, 1.7)$ is divided into two bins and the divided positions z_1 is set to 1.0. The figure of merit for each case is also included.

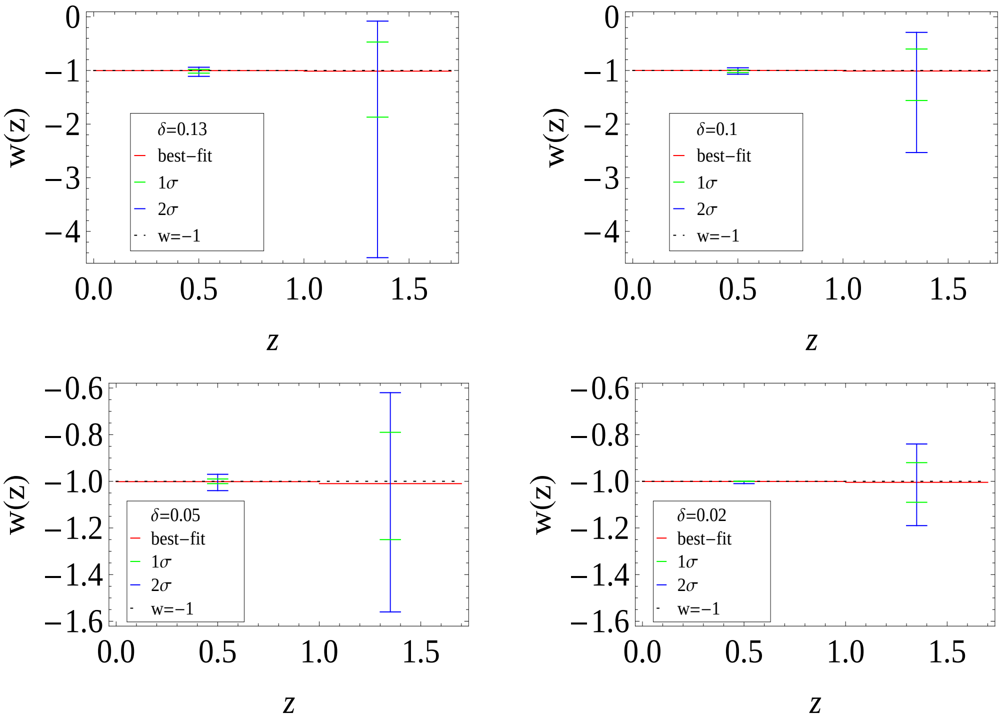

FIG. 5: Plots of the best-fitted $w_{de}(z)$ and their 68.3% and 95.4% C.L. errors shown in Table VII.

will be 3 times of the elementary data and $z_1 = 1.0$ is set. The results show in Table VII that FoM increases very rapidly with the decrease of δ. For example, as $\delta = 0.02$, the constraints of w_{de} in $z \in (1, 1.7)$ is even better than the present constraints of w_{de} at low redshift bin obtained in previous section. Moreover, w_{de} at the low redshift region can be definitively determined with $\delta = 0.02$, as shown in Table VII.

IV. SUMMARY

We have used the UBE method to estimate the limitations in determining w_{de} at high redshift from current and future mock supernovae data. The redshift region of the data points is divided into two bins with the divided position z_1. Best-fitted w_1, w_2 and their errors at 68.3%, 95.4% C.L. are obtained by using the MCMC method. FoM for each case is also calculated, which can be used to estimate goodness of constraints on w_2. Constraints on w_2 represent the ability of observational data in determining w_{de} beyond $z = z_1$.

For the present observational data set, 472 Supernovae Legacy Survey 3 years data, BAO Distance Parameter A, and 12 Observational Hubble data with $z < 1.4$ are adopted. It has been shown that the errors of w_2 increase rapidly with the divided position z_1. For the current observational data, the constraints of w_{de} beyond roughly $z = 0.3$ are still very weak. The downward errors of w_{de} at high redshift are extremely large, since the likelihood of w_{de} at high redshift is very flat on the downward side.

For the future data, we have simulated supernovae data from a SNAP-like JDEM survey. The effects of divided position z_1, the number of supernovae data points and the error in the distance modulus are analyzed. It was shown that the constraints of w_{de} from the mock 2298 supernovae data are extremely weak beyond roughly $z = 1$. The increase of the number of supernovae data seems not as efficient as the decrease of the error of distance modulus in improving constraints of w_{de} at high redshift.

Nowadays, many projects for the observations of DE are in progress or in planning, it is expected that a great deal of data points would be released. The observation from supernovae is still the most important one to reveal the behavior of DE. To make sure whether w_{de} is dynamical or not, a narrow constraint of w_{de} at high redshift is required. We need much more data points, and the improvement of accuracy of the observations seems more necessary. It is shown in Table VII that ~ 6900 SnIa data with their observational errors $\sigma = 0.02$ will constrain uncertainties of w_{de} beyond $z = 1$ within 0.1 at 68.3% C.L. and within 0.2 at 95.4% C.L. . Note that all observations used and analyzed in this paper relate to the distance measurement. Obviously it is believed that more observations of other types for DE combining with distance measurements should improve the constraints of w_{de}

at high redshift.

Acknowledgements:

This work was supported in part by the National Natural Science Foundation of China (No.10821504, No.10975168, No.11035008 and No.11147186), in part by the Ministry of Science and Technology of China under Grant No. 2010CB833004, and a grant from Hanzhou Normal University.

[1] A. G. Riess *et al.* [Supernova Search Team Collaboration], Astron. J. **116** (1998) 1009 [astro-ph/9805201].

[2] S. Perlmutter *et al.* [Supernova Cosmology Project Collaboration], Astrophys. J. **517** (1999) 565 [astro-ph/9812133].

[3] P. J. E. Peebles and B. Ratra, Rev. Mod. Phys. **75** (2003) 559 [astro-ph/0207347].

[4] E. J. Copeland, M. Sami and S. Tsujikawa, Int. J. Mod. Phys. D **15** (2006) 1753 [hep-th/0603057].

[5] P. J. Steinhardt, L. -M. Wang and I. Zlatev, Phys. Rev. D **59** (1999) 123504 [astro-ph/9812313].

[6] S. Capozziello, S. Carloni and A. Troisi, Recent Res. Dev. Astron. Astrophys. **1** (2003) 625 [astro-ph/0303041].

[7] R. -G. Cai, Phys. Lett. B **657** (2007) 228 [arXiv:0707.4049 [hep-th]].

[8] R. -G. Cai and Q. Su, Phys. Rev. D **81** (2010) 103514 [arXiv:0912.1943 [astro-ph.CO]].

[9] R. -G. Cai, Z. -L. Tuo, H. -B. Zhang and Q. Su, Phys. Rev. D **84** (2011) 123501 [arXiv:1011.3212 [astro-ph.CO]].

[10] M. Chevallier and D. Polarski, Int. J. Mod. Phys. D **10** (2001) 213 [gr-qc/0009008].

[11] E. V. Linder, Phys. Rev. Lett. **90** (2003) 091301 [astro-ph/0208512].

[12] A. R. Cooray and D. Huterer, Astrophys. J. **513** (1999) L95 [astro-ph/9901097].

[13] D. Huterer and M. S. Turner, Phys. Rev. D **64** (2001) 123527 [astro-ph/0012510].

[14] D. Huterer and G. Starkman, Phys. Rev. Lett. **90** (2003) 031301 [astro-ph/0207517].

[15] D. Huterer and A. Cooray, Phys. Rev. D **71** (2005) 023506 [astro-ph/0404062].

[16] Y. Wang, Phys. Rev. D **80** (2009) 123525 [arXiv:0910.2492 [astro-ph.CO]].

[17] T. Holsclaw, U. Alam, B. Sanso, H. Lee, K. Heitmann, S. Habib and D. Higdon, Phys. Rev.

D **82** (2010) 103502 [arXiv:1009.5443 [astro-ph.CO]].

[18] S. Sullivan, A. Cooray and D. E. Holz, JCAP **0709** (2007) 004 [arXiv:0706.3730 [astro-ph]].

[19] G. -B. Zhao, D. Huterer and X. Zhang, Phys. Rev. D **77** (2008) 121302 [arXiv:0712.2277 [astro-ph]].

[20] P. Serra, A. Cooray, D. E. Holz, A. Melchiorri, S. Pandolfi and D. Sarkar, Phys. Rev. D **80** (2009) 121302 [arXiv:0908.3186 [astro-ph.CO]].

[21] R. -G. Cai, Q. Su and H. -B. Zhang, JCAP **1004** (2010) 012 [arXiv:1001.2207 [astro-ph.CO]].

[22] A. Hojjati, L. Pogosian and G. -B. Zhao, JCAP **1004** (2010) 007 [arXiv:0912.4843 [astro-ph.CO]].

[23] Q. Su, X. He and R. -G. Cai, arXiv:1204.2146 [astro-ph.CO].

[24] A. Conley, J. Guy, M. Sullivan, N. Regnault, P. Astier, C. Balland, S. Basa and R. G. Carlberg *et al.*, Astrophys. J. Suppl. **192** (2011) 1 [arXiv:1104.1443 [astro-ph.CO]].

[25] D. J. Eisenstein *et al.* [SDSS Collaboration], Astrophys. J. **633** (2005) 560 [astro-ph/0501171].

[26] A. G. Riess, L. Macri, S. Casertano, H. Lampeitl, H. C. Ferguson, A. V. Filippenko, S. W. Jha and W. Li *et al.*, Astrophys. J. **730** (2011) 119 [Erratum-ibid. **732** (2011) 129] [arXiv:1103.2976 [astro-ph.CO]].

[27] D. Stern, R. Jimenez, L. Verde, M. Kamionkowski and S. A. Stanford, JCAP **1002** (2010) 008 [arXiv:0907.3149 [astro-ph.CO]].

[28] E. Gaztanaga, A. Cabre and L. Hui, Mon. Not. Roy. Astron. Soc. **399** (2009) 1663 [arXiv:0807.3551 [astro-ph]].

[29] Y. Wang, Phys. Rev. D **77** (2008) 123525 [arXiv:0803.4295 [astro-ph]].

[30] Q. Su, Z. -L. Tuo and R. -G. Cai, Phys. Rev. D **84** (2011) 103519 [arXiv:1109.2846 [astro-ph.CO]].

[31] A. G. Kim, E. V. Linder, R. Miquel and N. Mostek, Mon. Not. Roy. Astron. Soc. **347** (2004) 909 [astro-ph/0304509].

[32] A. Ealet *et al.* [SNAP Collaboration], [astro-ph/0210087].

[33] I. Maor, R. Brustein and P. J. Steinhardt, Phys. Rev. Lett. **86** (2001) 6 [Erratum-ibid. **87** (2001) 049901] [astro-ph/0007297].

[34] D. H. Weinberg, M. J. Mortonson, D. J. Eisenstein, C. Hirata, A. G. Riess and E. Rozo, arXiv:1201.2434 [astro-ph.CO].